BEHAVIOR OF PULTRUDED GFRP COLUMNS

Daniel Cardoso

dctcardoso@puc-rio.br

Pontificia Universidade Catolica do Rio de Janeiro (PUC-Rio), Dept. of Civil Engineering

R. Marques de Sao Vicente, 225 – Gavea, 22451-900, Rio de Janeiro, RJ, Brazil

Eduardo Batista

batista@coc.ufrj.br

COPPE / Federal University of Rio de Janeiro (UFRJ), Civil Engineering Program

Centro de Tecnologia, Bloco B – Cidade Universitaria, PB 68506, 21945-972, Rio de Janeiro RJ, Brazil

Abstract. *Pultruded members of glass-fiber reinforced polymer (GFRP) have been increasingly used in construction, especially because of their elevated strength / weight ratio and good performance in aggressive environments if compared to traditional building materials. Pultruded GFRP has a compressive strength similar to mild structural steel. On the other hand, longitudinal modulus of elasticity is low and the combination of very low modulus-to-strength ratio with the use of slender sections subject to compression leads to important instability problems that. This issue is aggravated by the considerably lower-still transverse and shear moduli, resulting from the mostly unidirectional reinforcement of GFRP This work aims to present a comprehensive approach to the behavior and strength of GFRP columns. A novel method to determine local buckling critical stresses and a theoretical model to predict compressive strength of real columns are presented. Local buckling expressions are validated numerically – using Finite Strip Method (FSM) – and experimentally. An experimental program on square tubes is also presented and the results are compared with a lower bound compressive strength curve.*

Keywords: *Glass-fiber reinforced polymer, Columns, Compressive strength*

1 INTRODUCTION

In the last 20 years, various authors have addressed the performance and strength of pultruded GFRP members subject to short term concentric compression and a significant number of works addressing global buckling, local buckling, buckling interaction and compressive strength of GFRP columns can be found. Additionally, large scale pultrusion of GFRP has contributed to reducing manufacturing costs, making these products competitive and significant efforts are underway worldwide to develop standard provisions for the design of GFRP structural members; these include the Eurocomp Design Code Handbook (CLARKE, 1996), the Italian Code (CNR, 2008) and the ASCE Pultruded Fiber Reinforced Polymer (FRP) Structures standard presently nearing completion. However, there remains a number of important gaps in the knowledge and understanding of the behavior of these members. Some of these gaps served as motivation for this work and are presented in the following paragraphs.

First of all, closed-form equations to determine critical loads for GFRP sections are very complicated and must accommodate a range of material properties and section geometries. To simplify such equations, existing design standards and manuals assume simply-supported edge conditions at wall intersections. This assumption leads to very conservative results. On the other hand, some expressions have been developed which demonstrate good agreement with numerical and experimental results, but these usually require enormous calculation effort and must typically be applied on a case-by-case basis rather than generalized in a design methodology. There is little consensus among researchers as to the best design approach for local buckling of GFRP sections, which needs to be both simple and accurate.

Specifically considering the compressive strength of GFRP columns, some explicit equations can be found in literature. However, these are typically empirical or have coefficients empirically determined primarily from observations of tested WF-sections. In this work, a theoretical model of a real column comprised of real constituent plates is developed and a rational compressive strength equation is derived.

At last, most of the previous works have focused on so-called ‘WF-sections’ (doubly-symmetric wide flange I-shaped sections generally with a flange width equal to their section depth). Little attention has been devoted to other section shapes despite their potential advantages as compression members. A square tube, for instance, has (i) a radius of gyration much greater than an I-shaped section with respect to the weakest axis, leading to an improved global buckling strength for a certain column length; (ii) the walls comprising the cross section are supported at both edges along the column length, which results in an enhanced local buckling strength; (iii) the internal void can be used for facilities; and (iv) improved aesthetics over open shapes. Despite the advantages, only a few works investigating the compressive performance of square tube columns, typically focusing on long column behavior, are available. Therefore, one motivation of this work arises from the necessity of extending this investigation to square tube compression members having different lengths and width-to-wall thickness ratios, resulting in a range of combinations of global and sectional slenderness.

2 PERFECT COLUMNS AND PLATES

The term ‘ideal’ or ‘perfect columns’ (PC) herein adopted is the one defined by TIMOSHENKO and GERE (1961): initially perfectly straight members subject to a concentric compression force. Similarly, the term ‘ideal’ or ‘perfect plates’ (PP) can be adopted for the study of plates subject to compression; these are initially perfectly flat and subject to concentric in-plane compression load.

In the case of a perfect column with a cross-section comprised of perfect plates (PC-PP), the following naturally uncoupled failure modes associated with the instability limit state may occur: global buckling and local buckling. Additionally, a third failure mode occurs if the column material compressive strength is exceeded (crushing) prior to global or local buckling.

2.1 Crushing

The term 'crushing' generally refers to all collapse modes that may occur at the constituent material level of a fibrous composite material: elastic microbuckling, plastic microbuckling and fiber crushing (FLECK, 1997). A closed-form equation for GFRP material crushing strength ($F_{L,c}$) was derived by BARBERO (1998) and BARBERO *et al*. (1999) based on a continuum damage model with fiber misalignment statistically distributed within the cross section. However, some input data for the method (specification of the material used for roving layers and their thickness) are rarely presented in data sheets, tables and manuals provided by manufacturers. Recently, CARDOSO *et al.* (2014a) proposed an empirical expression based on linear regression of mean experimental results obtained by various authors (Eq. 1):

$$F_{L,c} = 191 + 352V_f \qquad \text{(in MPa)} \tag{1}$$

in which V_f is the fiber content in volume.

2.2 Global Buckling

Global buckling includes the following buckling modes: flexural, torsional and flexural-torsional. In the available literature, major effort has been directed toward global buckling of doubly symmetric sections, with little attention devoted to monosymmetric or asymmetric cross-sections (HEWSON, 1978, ZUREICK AND STEFFEN, 2000).

For flexural buckling, available standards and design manuals (GRAY, 1984, CLARKE, 1996, CNR, 2008) adopt Euler equation to predict the global buckling critical stress of GFRP columns, $F_{crg,F}$. However, although validated by experiments with slender columns (BARBERO and TOMBLIN, 1993, ZUREICK and SCOTT, 1997), Euler equation does not take into account the shear effect, which is important for materials with very low in-plane shear modulus such as GFRP (ZUREICK and SCOTT, 1997, LANE and MOTTRAM, 2002). To address this issue, an accurate equation derived by TIMOSHENKO and GERE (1961) is recommended to determine the global buckling critical stress (Eq. 2):

$$F_{crg,F} = \frac{\sqrt{1 + 4n_s F_e / G_{LT}} - 1}{2n_s / G_{LT}} \tag{2}$$

in which $F_e = \pi^2 E_L/(K_e L/r)^2$ is the Euler critical buckling stress; E_L is the cross-sectional flexural modulus of elasticity; K_eL is the column effective length; r is the radius of gyration; n_s is the form factor for shear; and G_{LT} is the in-plane shear modulus of the section.

2.3 Local Buckling

To analytically determine the local buckling stress of columns subjected to concentric compression, three different approaches may be used, as described below:

i) buckling analysis of individual plates without interaction between plate elements: this approach is based on the assumption of simply-supported conditions at the plate intersections junction and has been adopted by most available standards (GRAY, 1984, CLARKE, 1996). The solution, obtained by LEKHNITSKII (1968), is essentially valid for long plates with both longitudinal edges simply-supported (SS) and one edge free and the other simply-supported (FS). This approach is often conservative.

ii) buckling analysis of individual plates rotationally restrained by adjacent plates: this approach was firstly introduced by BLEICH (1952) and has been adopted by many authors to develop comprehensive closed-form expressions for local buckling of pultruded sections (BANK and YIN, 1996, QIAO et al., 2001, KOLLAR, 2002, 2003, QIAO and SHAN, 2005). In general, expressions obtained by these authors showed good agreement with numerical predictions and Kollar's equations were included in an appendix of the Italian standard (CNR, 2008) to specifically address the local buckling of I-sections. Although accurate, these equations require independent calculations for each constituent plate of the cross section and the calculation of section-specific parameters, such as the elastic restraint coefficient, substantially increase calculation effort.

iii) full section buckling analysis with appropriate continuity conditions at plate intersections: early attempts were made to develop expressions and design charts to determine the local buckling coefficients for steel sections (LUNDQUIST, 1943, KROLL, 1943, CRCJ, 1971). CARDOSO *et al.* (2014c) used the Rayleigh Quotient energy method along with approximate deflected-shapes to determine an expression for the local buckling critical stress $F_{cr\ell}$ (Eq. 3) and a set of equations for the local buckling coefficient k_{cr} (Table 1) of infinitely long columns with typical cross sections made of orthotropic material. The cross sections adopted in this study are also described in Table 1.

$$F_{cr\ell} = k_{cr}\,\frac{\pi^2 E_{L,f}}{12\left(1-\nu_{LT}\nu_{TL}\right)}\left(\frac{t}{b_w}\right)^2 \tag{3}$$

where $E_{L,f}$ is the plate flexural modulus of elasticity in the longitudinal direction; ν_{LT} and ν_{TL} are major and minor Poisson's ratio, respectively; b_w is the web width; and t its thickness.

Table 1. Local buckling coefficients for typical cross sections made of orthotropic material

Cross-section	Local buckling coefficient
Angle	$k_{cr} = \frac{12(1+\eta)}{\pi^2(1+\eta^3)}(1-\nu_{LT}\nu_{TL})\frac{G_{LT}}{E_{L,f}}$
Channel	$k_{cr} = \frac{2}{\sqrt{1+4\pi^2\eta^3/3}}\sqrt{\frac{E_{T,f}}{E_{L,f}}} + \frac{2\nu_{LT}\frac{E_{T,f}}{E_{L,f}} + 4(1+4\eta)(1-\nu_{LT}\nu_{TL})\frac{G_{LT}}{E_{L,f}}}{(1+4\pi^2\eta^3/3)}$
I-section	$k_{cr} = \frac{2}{\sqrt{1+\pi^2\eta^3/3}}\sqrt{\frac{E_{T,f}}{E_{L,f}}} + \frac{2\nu_{LT}\frac{E_{T,f}}{E_{L,f}} + 4(1+4\eta)(1-\nu_{LT}\nu_{TL})\frac{G_{LT}}{E_{L,f}}}{(1+\pi^2\eta^3/3)}$
Rectangular tube $0{,}25 \le \eta \le 1{,}0$	$k_{cr} = 2\sqrt{3.4-2.4\eta}\sqrt{\frac{E_{T,f}}{E_{L,f}}} + (0.81+1.32\eta-1.13\eta^2)\left[2\nu_{LT}\frac{E_{T,f}}{E_{L,f}} + 4(1-\nu_{LT}\nu_{TL})\frac{G_{LT}}{E_{L,f}}\right]$

*$E_{T,f}$ is the plate flexural modulus of elasticity in the transverse direction; $\eta = b_f/b_w$; b_f is the flange width.

To validate the analytical approach, CARDOSO *et al.* (2014c) compared the proposed buckling coefficients for typical cross sections with those obtained with Finite Strip Method (FSM) (implemented using CUFSM 4.04 (LI and SCHAFER, 2010)). Figure 1 presents graphs for each cross section where k_{cr} is plotted against the flange-to-web width ratio ($\eta = b_f/b_w$), considering isotropic and two different orthotropy conditions: i) $E_{L,f}/E_{T,f}$ = 1,0 e $E_{L,f}/G_{LT}$ = 3,5; ii) $E_{L,f}/E_{T,f}$ = 2,0 e $E_{L,f}/G_{LT}$ = 6,5. Lekhnitskii's equations (simply-supported conditions at junctions) are plotted along for the case ii) of orthotropy.

A summary of the resulting equations, their range of applicability in terms of b_f/b_w and the observed relative differences of the various values of k_{cr} from those obtained using finite strip method (FSM) is presented in Table 2. The observed differences between FSM and the equations promulgated in current standards and guidelines (Lekhnitskii's equations) are also shown. While the proposed method is in good agreement with the actual behavior, Lekhnitskii's equations lead to very conservative results.

Table 2. Differences observed between Eq.3 and FSM and between Lekhnitskii's equations and FSM.

Cross-section	Applicable b_f/b_w *	Greatest relative difference from FSM solution in range of applicability	
		Proposed Method (Eq. 3)	Lekhnitskii (1968)
Angle	$0{,}33 \leq \eta \leq 1{,}0$	1%	25%
Channel	$0{,}45 \leq \eta \leq 1{,}05$	10%	55%
I-section	$0{,}15 \leq \eta \leq 0{,}53$	6%	49%
Rectangular tube	$0{,}25 \leq \eta \leq 1{,}0$	3%	32%

*Applicable b_f/b_w refers to the geometry of typical commercially-available sections.

3 REAL COLUMNS

Real columns (RC) are those affected by geometric and material imperfections, where applied compressive force produces second-order bending moments that result in increased lateral deflections and therefore reduced critical capacities compared to those described for 'perfect' columns. A similar behavior is observed for real plates (RP). In the case of a real column comprised of real plates (RC-RP), compressive capacity is affected by second-order effects on both column and constituent plates; in this case failure occurs when the compressive stress at the most compressed face of a certain plate equals the material strength. RC-RP constitutes a coupled buckling problem and may lead to significant reduction of load-carrying capacity (BATISTA, 2004). The degree of interaction between these buckling modes is dependent on the initial imperfections and can be accurately obtained from a non-linear analysis considering initial imperfections and post-buckling behavior.

The first attempt to develop a compressive strength curve for GFRP columns taking into account buckling interaction was made by BARBERO and TOMBLIN (1994), who observed that the failure loads of I-shaped intermediate columns were as much as 25% lower than theoretical critical loads, demonstrating that coupled buckling significantly affects capacity. The authors proposed an empirical equation for the ultimate strength of the column, F_u, based on ZAHN's (1992) universal equation for wood design. The equation was later revised by BARBERO and DE VIVO (1999) to include additional experimental data and is currently adopted by the Italian code (CNR, 2008). Alternative compressive strength equations were proposed by PUENTE *et al.* (2006) and SEAGATITH and SRIBOONLUE (1999), but none consider the influence of plate slenderness.

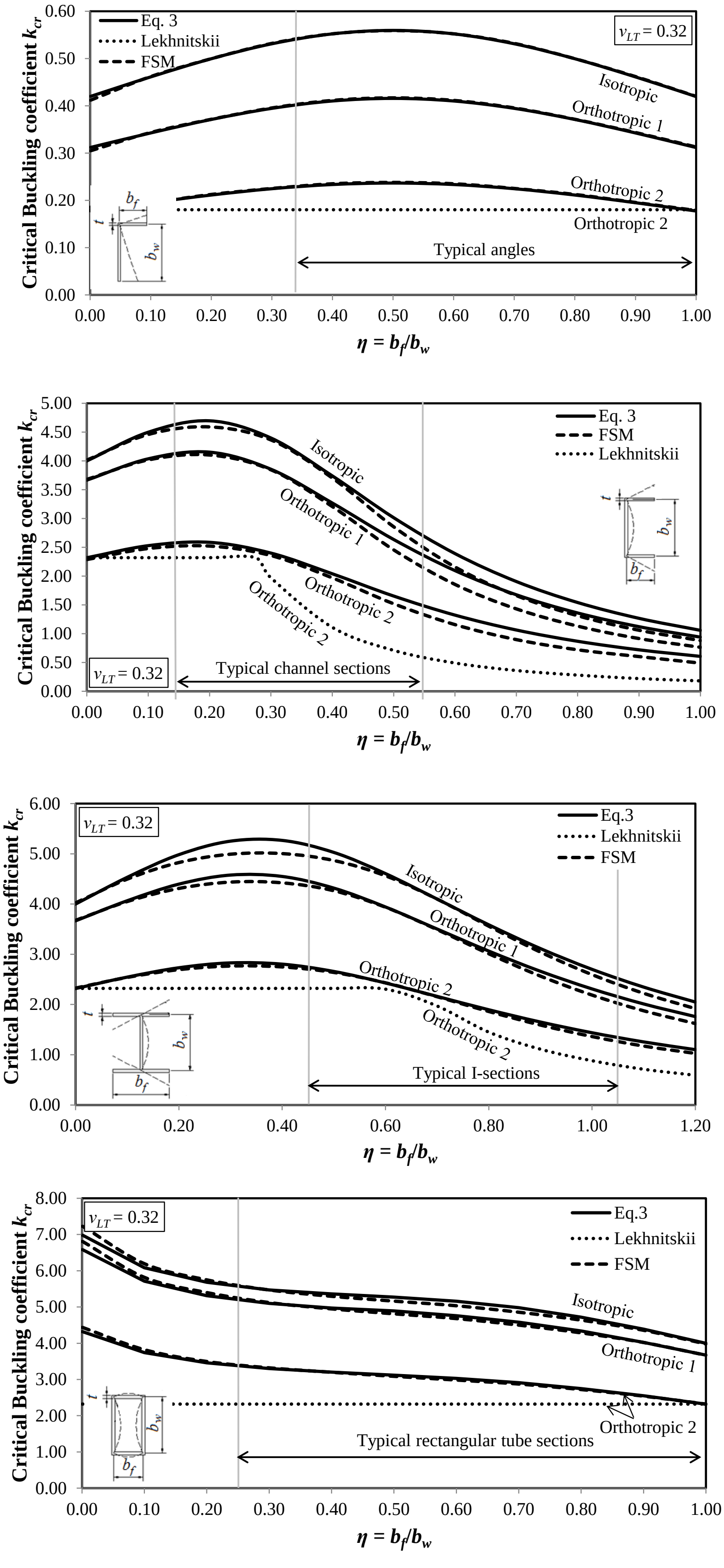

Figure 1. Local buckling coefficient, k_{cr}, versus $\eta = b_f/b_w$ for different cross sections.

To obtain a comprehensive strength curve, a theoretical model is developed and a simple methodology is presented in the subsequent sections.

3.1 Real Plate (RP)

The real plate theoretical model herein developed is similar to the one developed by CARDOSO *et al.* (2014b), which is based on the following assumptions: i) classical plate theory hypotheses apply; ii) stretching in the middle plane and post-buckling behavior are neglected; iii) the material behavior is linear elastic; iv) mechanical properties and thickness are uniform throughout the plate; v) residual stresses are negligible; vi) the initially deflected surface, w_0, is described by a double sinusoidal function: $w_0 = \Delta_0 \sin(\pi x/\ell_{cr}) \sin(\pi y/b)$, where L and b are the plate length and width, respectively, ℓ_{cr} is the half-waves length, Δ_0 is the out-of-flatness amplitude, and x and y are the in-plane axes (Figure 2); and failure criterion governed by maximum stress. Since the material has reported compressive and flexural strengths, the strength under combined axial-bending in the longitudinal direction, $F_{L,cf}$, is given as shown in Eq. 4:

$$F_{L,cf} = F_{L,f} - \frac{F_{L,f} - F_{L,c}}{F_{L,c}} \sigma_{x,c} \tag{4}$$

where $F_{L,f}$ and $F_{L,c}$ are the pure flexural and compressive strengths, respectively; and $\sigma_{x,c} = N_x/t$ is the compressive stress induced by the applied compressive load per unit of width acting in the x direction, N_x.

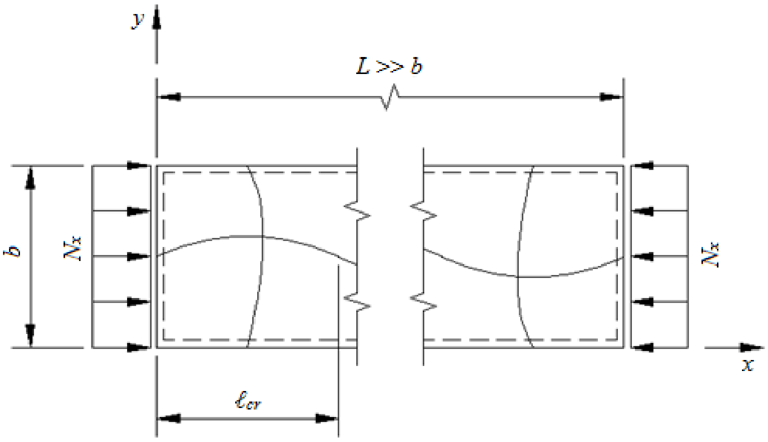

Figure 2. Uniaxially compressed plate with simply-supported conditions along the edges.

From classical plate theory (CPT) (TIMOSHENKO and GERE, 1961), it can be demonstrated that the additional out-of-plane deflection w is proportional to the initially deflected surface, $w = w_0\, \sigma_{x,c}/(F_{cr\ell}-\sigma_{x,c})$, and that the bending moment in the longitudinal direction per unit of width of plate, M_x, is given according to Eq. 5:

$$M_x = -\left(D_{11} \frac{\partial^2 w}{dx^2} + D_{12} \frac{\partial^2 w}{dy^2} \right) = w_0 \frac{\pi^2}{b^2} \left(D_{11} \frac{b^2}{\ell_{cr}^{\;2}} + D_{12} \right) \frac{\sigma_{x,c}}{F_{cr\ell} - \sigma_{x,c}} \tag{5}$$

in which $D_{11} = E_{L,f}\, t^3 / [12\,(1 - \nu_{12}\, \nu_{21})]$; $D_{22} = E_{T,f}\, t^3 / [12\,(1 - \nu_{12}\, \nu_{21})]$; $D_{12} = \nu_{12}\, D_{22}$; and $D_{66} = G_{12}\, t^3 / 12$ are plate stiffness parameters.

For a rectangular plate with all edges simply-supported, $\ell_{cr} = b(D_{22}/D_{11})^{1/4}$ and $F_{cr\ell} = \pi^2\, [\, 2(D_{11}D_{22})^{1/2} + 2D_{12} + 4D_{66}] / (b^2\, t)$. Furthermore, the maximum bending moment occurs at $x = \ell_{cr}/2$ and $y = b/2$, where $w_0 = \Delta_0$. In this case, the maximum compressive stress due to combined axial and bending moment in the section, $\sigma_{x,cf}$, is given as (Eq.6):

$$\sigma_{x,cf} = \sigma_{x,c} + \frac{6M_{x,max}}{t^2} = \sigma_{x,c} + 6\left(\frac{\Delta_0}{b}\right)\left(\frac{b}{t}\right)\left(\frac{D_{11}\sqrt{D_{11}/D_{22}} + D_{12}}{2\sqrt{D_{11}D_{22}} + 2D_{12} + 4D_{66}}\right)\frac{\sigma_{x,c}}{1-\sigma_{x,c}/F_{cr\ell}} \quad (6)$$

Considering that compressive stress $\sigma_{x,c}$ is increased to a limit a $F_{u,L}$ ($\sigma_{x,cf} = F_{L,cf}$):

$$F_{L,f} - \frac{F_{L,f} - F_{L,c}}{F_{L,c}} F_{u,L} = F_{u,L} + 6\left(\frac{\Delta_0}{b}\right)\left(\frac{b}{t}\right)\left(\frac{D_{11}\sqrt{D_{11}/D_{22}} + D_{12}}{2\sqrt{D_{11}D_{22}} + 2D_{12} + 4D_{66}}\right)\frac{F_{u,L}}{1-F_{u,L}/F_{cr\ell}} \quad (7)$$

Eq. 7 can be rearranged and written in terms of non-dimensional parameters (Eq. 8):

$$\lambda_p^2 \chi_p^2 - \left(1 + \alpha_{pL} + \lambda_p^2\right)\chi_p + 1 = 0 \quad (8)$$

where $\lambda_p = (F_{L,c}/F_{cr\ell})^{1/2}$ is the relative plate slenderness; $\chi_{p,L} = F_{u,L}/F_{L,c}$ is the normalized plate strength in the longitudinal direction; and the plate imperfection parameter, $\alpha_{p,L}$, is given in Eq. 9:

$$\alpha_{p,L} = 6\left(\frac{\Delta_0}{b}\right)\left(\frac{b}{t}\right)\frac{F_{L,c}}{F_{L,f}}\left(\frac{D_{11}\sqrt{D_{11}/D_{22}} + D_{12}}{2\sqrt{D_{11}D_{22}} + 2D_{12} + 4D_{66}}\right) \quad (9)$$

Eq. 9 can be solved in terms of the normalized plate strength $\chi_{p,L}$, resulting in:

$$\chi_{p,L} = \frac{1 + \alpha_{p,L} + \lambda_p^2 - \sqrt{\left(1 + \alpha_{p,L} + \lambda_p^2\right)^2 - 4\lambda_p^2}}{2\lambda_p^2} \quad (10)$$

Eq. 10 has the same form as the typical column strength curves developed for steel, such as those defined by Perry-Robertson (ZIEMIAN, 2010) and DUTHEIL (1961), with the imperfection factor in the longitudinal direction $\alpha_{p,L}$ defined as a function of geometry, initial imperfection, plate stiffness and strength parameters (Eq. 9). For other boundary conditions, different expressions for $\alpha_{p,L}$ are obtained, although these always depend on the same parameters. For $\alpha_{p,L} = 0$, the problem simplifies to the perfect plate condition, with $\chi_{p,L} = 1.0$ for $\lambda_p \leq 1.0$ and $\chi_{p,L} = 1/\lambda_p^2$ for $\lambda_p > 1.0$. Failure may also be initiated by the bending moment in the transverse direction, which can be investigated in a similar manner. For typical GFRP material properties and imperfection magnitudes, calculations have shown the strength is not significantly affected in this case.

The plate strength reduction factor ρ_p, representing the reduced capacity with respect to the perfect condition, is defined as the ratio of real-to-perfect plate normalized strengths:

$$\rho_p = \frac{\chi_p}{\chi_{p0}} \quad (11)$$

where χ_{p0} is the PP normalized strength: $\chi_{p0} = 1.0$ for $\lambda_p \leq 1.0$ and $\chi_{p0} = 1/\lambda_p^2$ for $\lambda_p > 1.0$.

3.2 Real Column Comprised of Real Plates (RC-RP)

The real column theoretical model herein developed is similar to the one developed by CARDOSO *et al.* (2014b), which is based on the following assumptions: i) beam column theory hypotheses apply; ii) the column bending stiffness remains constant until failure; iii) the initial deflected shape (out-of-straightness), v_0, is described by a sinusoidal function: $v_0 = \delta_0 \sin(\pi x/L)$, where x is the longitudinal axis of a column of length L and δ_0 is the amplitude of the initial out-of-straightness; iv) the initial eccentricities, e_0, is equal at both ends; v) failure occurs when the compressive stress at a certain plate comprising the cross-section reaches its ultimate compressive stress, $F_{u,L} = \chi_{p,L}F_{L,c} = \rho_p F_{PP}$, in which F_{PP} is the PP strength, given as the lesser of $F_{c,L}$ and $F_{cr\ell}$.

From beam-column theory (TIMOSHENKO and GERE, 1961), it can be shown that the maximum bending moment M_{max} for a compressed column with initial out-of-straightness, δ_0, and eccentricity, e_0, is:

$$M_{\max} = \frac{\sigma_c A}{1-\sigma_c / F_{crg}}\left[e_0\left(1+\frac{4}{\pi}\frac{\sigma_c}{F_{crg}}-\frac{\sigma_c}{F_{crg}}\right)+\delta_0\right] \tag{12}$$

in which σ_c is the compressive stress applied; A is the cross-sectional area; and F_{crg} is the global buckling critical stress given by Eq. 2. In Eq. 12, the term in parenthesis that modifies e_0 ranges from 1.0 to approximately $4/\pi$ as σ_c varies from 0 to F_{crg}. Conservatively setting this term equal to $4/\pi$, the the maximum compressive stress at an outer fiber of the column is:

$$\sigma_{c,\max} = \sigma_c + \frac{\sigma_c}{\left(1-\sigma_c / F_{crg}\right)}\frac{A}{S}\left(\frac{4}{\pi}e_0+\delta_0\right) \tag{13}$$

where S is the elastic section modulus.

Increasing the compressive stress σ_c to a limit of F_u when failure occurs ($\sigma_{c,max} = \rho_p F_{PP}$):

$$\rho_p F_{PP} = F_u + \frac{F_u}{\left(1-F_u / F_{crg}\right)}\frac{A}{S}\left(\frac{4}{\pi}e_0+\delta_0\right) \tag{14}$$

Eq. 14 can be rearranged and written in terms of non-dimensional parameters:

$$\lambda_c^2\chi_c^2 - \left(1+\alpha_c+\lambda_c^2\rho_p\right)\chi_c + 1 = 0 \tag{15}$$

in which $\lambda_c = (F_{PP}/F_{crg})^{1/2} = [\min(F_{L,c}, F_{cr\ell})/F_{crg}]^{1/2}$ is the relative column slenderness; $\chi_c = F_u/F_{PP}$ is the normalized column strength in the longitudinal direction; and α_c is the imperfection factor given as:

$$\alpha_c = \left(\frac{4}{\pi}e_0+\delta_0\right)\frac{A}{S} \tag{16}$$

Eq. 16 can be solved in terms of the normalized column strength χ_c, resulting in:

$$\chi_c = \frac{1+\alpha_c+\lambda_c^2\rho_p - \sqrt{\left(1+\alpha_c+\lambda_c^2\rho_p\right)^2 - 4\lambda_c^2}}{2\lambda_c^2} \tag{17}$$

The column capacity reduction factor ρ_c, representing the residual capacity with respect to the ideal condition (PC-PP), can be defined as:

$$\rho_c = \frac{\chi_c}{\chi_{c0}} \tag{18}$$

where χ_{c0} is the PC-PP normalized strength: χ_{c0} = 1.0 for $\lambda_c \leq 1.0$ and $\chi_{c0} = 1/\lambda_c^2$ for $\lambda_c > 1.0$.

Figure 3 shows examples of representative column strength curves taking into account the interaction between plate and column behavior. It can be seen that maximum reduction of capacity occurs for $\lambda_c = 1$ and that, for a relative slenderness $\lambda_c = 0$, the normalized strength is less than 1.0, reflecting the initial eccentricity and its resulting first order bending moment.

An important conclusion of the study is that the strength can be expressed as a function of two variables: relative column and plate slenderness (λ_c and λ_p, respectively).

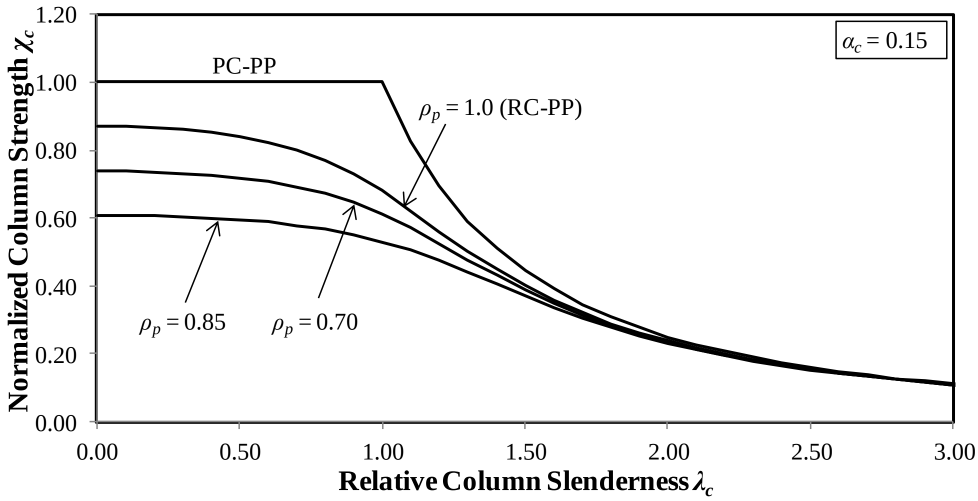

Figure 3. Normalized column strength vs. relative column slenderness for different plate strength reduction factors.

4 LOCAL BUCKLING TESTS ON I-SECTIONS

In this section, a summary of the experimental program conducted by CARDOSO *et al.* (2015) is presented. The aim of the work was to validate experimentally Eq. 3.

Pultruded GFRP I-sections made with both polyester (PE) and vinyl ester (VE) matrices were tested. Different flange width-to-section depth ratios (b_f/d) and flange width-to-thickness (b_f/t) were considered: 102x(102-51)x6.4 mm and 76x(76-38)x6.4 mm, where designation refers to the nominal depth (d) x flange width (b_f) x wall thickness (t). The experimental program was conducted in three stages: geometry measurements, material characterization and compression tests. No significant geometry deviations were observed within a cross-section. Sections were provided by the same manufacturer and flange/web plates have same thickness and similar fiber architecture. Material properties obtained are presented in Table 3.

Table 3 – Experimental material properties.

Resin	F_c (MPa)	$E_{L,c}$ (MPa)	E_L (MPa)	E_T (MPa)	G_{LT} (MPa)	E_L/E_T	E_L/G_{LT}	$E_L/E_{L,c}$
VE	453	27,066	23,091	11,777	4549	1.96	5.08	0.85
PE	294	27,314	20,695	8760	3811	2.36	5.43	0.76

A total of 36 stub columns with b_f/d ranging from 0.5 to 1.0 were tested in concentric compression under displacement control at a rate of 0.10 mm/min. Stub columns with b_f/d = 1.0 and 0.75 were instrumented with two back-to-back uniaxial strain gauges (with their sensitive axes parallel to the stub column's axis) located close to the edge of the flange to coincide with the peak of the idealized buckled shape. For stub columns with b_f/d = 0.5, the strain gages were located on the web, since the flanges are very narrow. Figure 4 presents views of representative tests.

a) b_f/d=0.99 length=400 mm (VE) | b) b_f/d=0.73 length=400 mm (PE) | c) b_f/d=0.48 length=266 mm (VE)

Figure 4. Representative compression tests on stub columns.

For each stub column tested, applied compressive stress and specific flexure deformation were correlated and the critical local buckling stresses, $F_{cr\ell}$, were obtained through Southwell plot (SOUTHWELL, 1932). More pronounced deflections were observed for sections 102x102x6.4 (b_f/d ~1,0), while much less pronounced deflections were observed for sections with b_f/d ~ 0,5, where the proximity of crushing strength ($F_{L,c}$) and critical stress led to failure before large deformations developed (Figs. 4a e 4c).

Figure 5 presents the experimentally determined local buckling coefficients, k, obtained by dividing the experimental critical stresses by $\pi^2 EL_{,f}/[12(1\text{-}\nu_{LT}\,\nu_{TL})](t/b_w)^2$, in which t is the average thickness. Curves for k_{cr} obtained from Lekhnitskii's equations and Eq. 3 are also shown. These were obtained for $E_{L,f}/E_{T,f}$ = 2.16 and $E_{L,f}/G_{LT}$ = 5.26, corresponding average properties of materials tested (Table 3). As expected, experimental results were greater than those predicted using Eq. 3, due to length and boundary conditions effect, which are important for short columns. Two exceptions were observed for stub columns with b_f/b_w ~ 0.5. Possible explanations are: i) inaccuracy of Southwell plots due to the occurrence of the instrumented section crushing prior to transverse deflection growth stabilization (resulting from the inability to locate the strain gage at the peak of an a priori unknown buckled shape); ii) reduction in the elastic properties due to the applied stresses having the same order of magnitude as the crushing stress; or iii) critical stresses may be affected by transverse shear which has been shown to be important when b/t < 13 (BARBERO, 2011). It can also be seen that the method recommended by current standards and guidelines are usually conservative.

In order to validate the proposed approach, the ratios of predicted-to-experimental critical stresses ($F_{cr\ell}/F_{cr\ell,exp}$) gathered from literature (TOMBLIN and BARBERO, 1994, TURVEY and ZHANG, 2004) and from the present study are presented in Figure 7. Predicted capacities are based on Lekhnitskii's equations and on the approach proposed in Eq. 3. The proposed equations indicate better correlation with the experimental results with the average ratio $F_{cr\ell}/F_{cr\ell,exp}$ = 0.86 ± 0.11, whereas the use of Lekhnitskii's equations leads to an average of

0.53 ± 0.16. Considering only such WF shapes (previous studies), the average ratios of predicted-to-experimental critical stresses calculated using Lekhnitskii's equations, fall to $F_{cr\ell}/F_{cr\ell,exp}$ = 0.48 ± 0.15, while the ratio based on Eq. 3 remains unchanged. Thus, it is demonstrated that considering only simply-supported junctions between web and flange plates results in underestimation of the buckling capacity of pultruded I-section stub columns and that the extent of the underestimation reduces as the flange slenderness b_f/d reduces. These facts, taken together, have implications for the 'calibration' of building code factors (φ-factors). Using Lekhnitskii's equations, reliability calibrations will result in high φ-factors which misrepresent the material reliability and may be appropriate for only WF shapes. Calibrations using Eq. 3 will result in 'representative' and uniformly applicable φ factors.

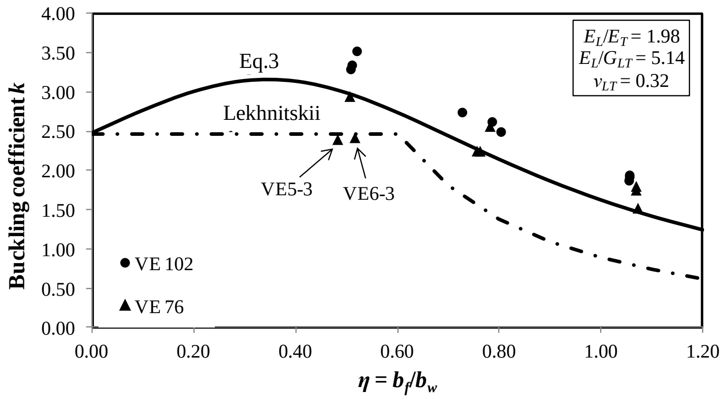

a) VE sections

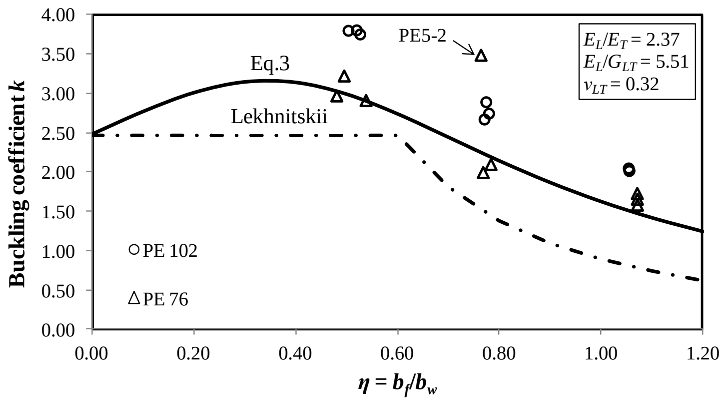

b) PE sections

Figure 5. Experimental and theoretical buckling coefficients k vs. bf/bw.

5 COMPRESSION TESTS ON SQUARE TUBES

In this section, a summary of the experimental program conducted by CARDOSO *et al.* (2014b) is presented. The aim of the work was to validate experimentally Eq. 17, as well as to determine aparent imperfection factors and characterize failure modes.

In the study, square tubes with the following nominal sections were tested in concentric compression: 25.4x3.2 mm, 50.8x3.2 mm, 76.2x6.4 mm, 88.9x6.4 mm and 101.6x6.4 mm. Based on the dimensions of the sections and mechanical properties of the materials, both summarised in Table 4, column lengths were determined in order to cover a range of slenderness values intended to result in long ($\lambda_c \leq 0.7$), intermediate ($0.7 < \lambda_c < 1.3$) and short columns ($\lambda_c \geq 1.3$). In all, 74 tests were conducted. A map with the distribution of tests according to combination of slenderness is presented in Figure 7, along with tests conducted by other authors.

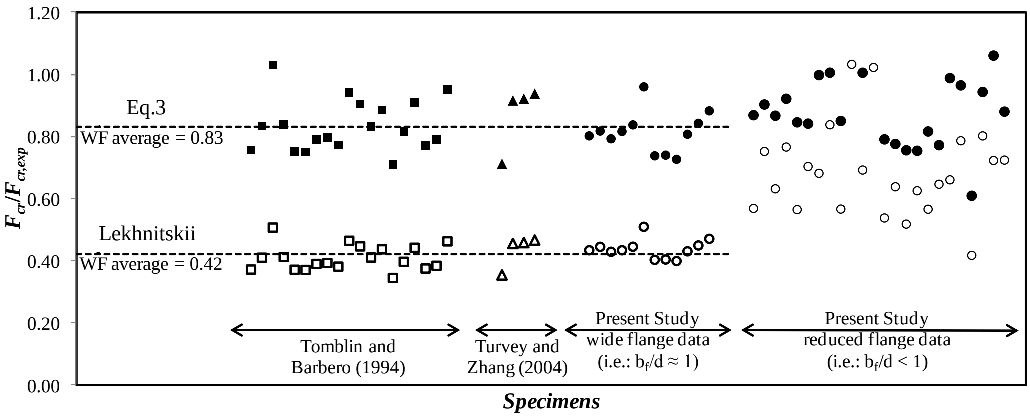

Figure 6. Ratios of predicted-to-experimental critical stresses from literature and present work.

Table 4. Cross-section dimensions, experimental material properties, predicted local buckling critical stresses and section classification.

	25,4x3,2	50,8x3,2	76,2x6,4	88,9x6,4	102x6,4
Measured Section Dimensions					
largura, *b* (mm)	25,5 ± 0.2	50,7 ± 0.2	75,9 ± 0.2	88,8 ± 0.3	100,9 ± 0.1
espessura, *t* (mm)	3,19 ± 0.29	2,88 ± 0.10	6,23 ± 0.28	6,20 ± 0.19	6,33 ± 0.21
Mechanical Properties					
$F_{c,L}$ (MPa)	224	240	333	320	302
$E_{L,c}$ (MPa)	22100	23700	31100	29900	28200
$E_{L,f}$ (MPa)	10800	11500	25000	24000	22700
$E_{T,f}$ (MPa)	9900	10500	13500	12800	12000
G_{LT} (MPa)	2100	2200	2700	2600	2400
ν_{LT}	0,33	0,33	0,32	0,32	0,33
Section Classification: compact ($\lambda_p \leq 0.7$), intermediate ($0.7 < \lambda_p < 1.3$) and slender ($\lambda_p \geq 1.3$)					
$F_{cr\ell}$ (MPa)	547	118	365	253	191
λ_p (Eq. 1)	0.64	1.43	0.95	1.12	1.26
Classification	compact	slender	intermediate	intermediate	intermediate

The columns were tested in concentric compression on a 900kN-capacity servo-hydraulic controlled universal test machine (Figure 8a). Rollers were located at both columns ends (Figure 8b) in order to reproduce one-dimensional pinned-pinned conditions. The tests were conducted under displacement control at a slow axial loading rate of approximately 750 με/min (based on initial specimen length). Tests were ended when either crushing was observed or the lateral deflection at midheight, Δ, exceeded L/50. In the latter case, the columns were unloaded at the same rate and retested in their other principle direction, if no damage was observed. The columns were instrumented with draw-wire transducers (DWT) to measure lateral deflections at midheight (Δ). The geometry of the rollers affects the column loading and end conditions. Due to the dimension of the roller, when the column deflects laterally, the line of action of the compressive force shifts, which causes a small restoring eccentricity. This condition is similar to the compression of bars with rounded ends (TIMOSHENKO and GERE, 1961) and is accounted for by means of an appropriately corrected effective length factor, K_e.

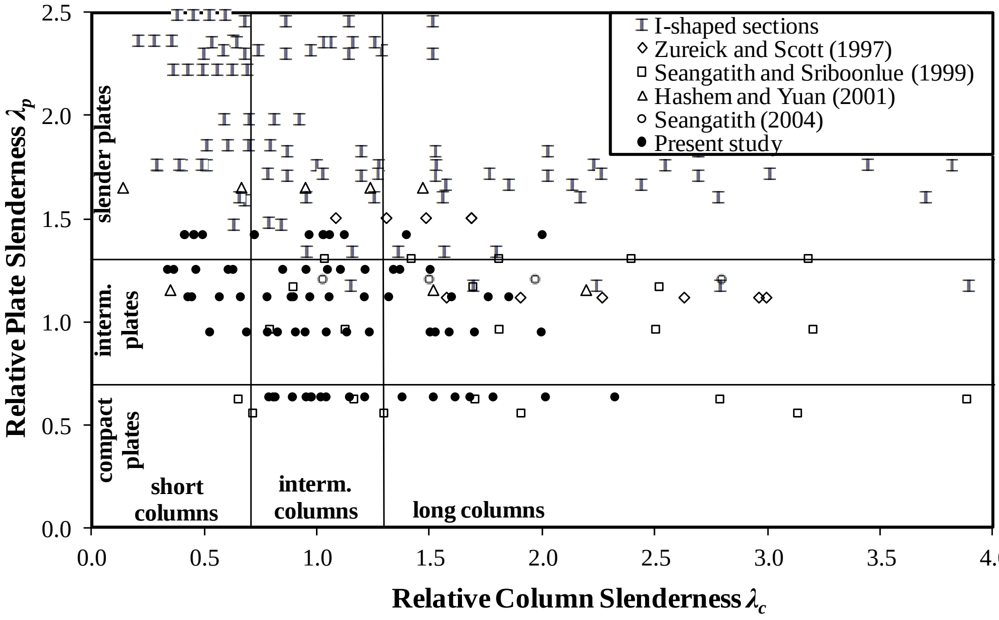

Figure 7. Summary of recent experimental works plotted according to plate and columns slenderness (specimens are hollow tubes except as indicated).

a) overall view of test set-up

b) one dimensional roller end condition

Figure 8. Column compression test set-up.

For each column tested, compressive stress and lateral deflections were correlated and the global buckling critical stresses, F_{crg}, were obtained experimentally from Southwell plots (SOUTHWELL, 1932). Figure 9 presents experimental and theoretical critical stresses (Eq. 2) normalized by the lesser between crushing strength, $F_{L,c}$, and local buckling critical stress, $F_{cr\ell}$, both presented in Table 4, plotted against the relative column slenderness λ_c (see Eq. 15). Similarly, normalized compressive strength, χ_c, obtained experimentally and theoretically (Eq. 2) are presented in Figure 10. From the figures, it can be noted that experimental results are in good agreement with the proposed lower bound strength curve (Eq. 17) for $\alpha_c = 0.34$ e $\rho_p = 0.92$, except for the long columns, where tests were interrupted for large lateral deflections and actual failure stresses were not achieved. α_c and ρ_p were experimentally determined and details about the methods adopted are presented in CARDOSO *et al.* (2014b).

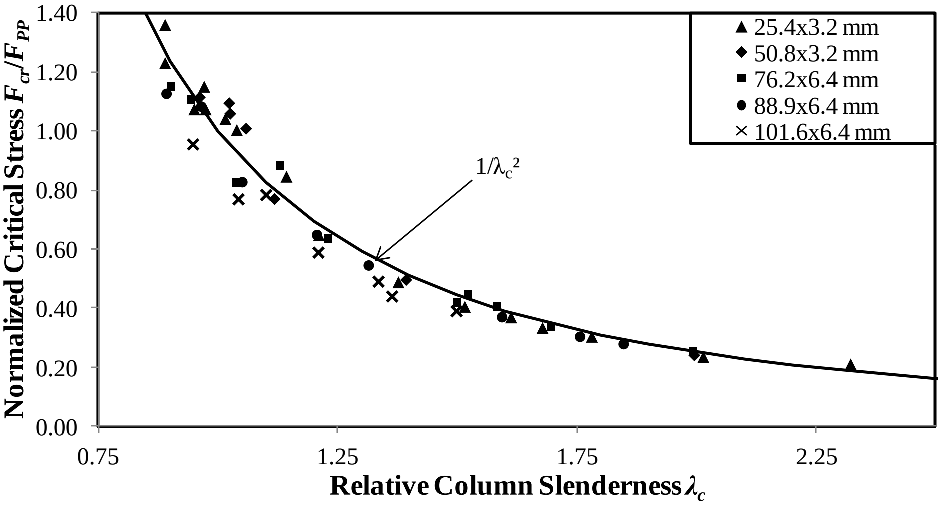

Figure 9. Experimental normalized critical stresses plotted against the relative column slenderness λ_c.

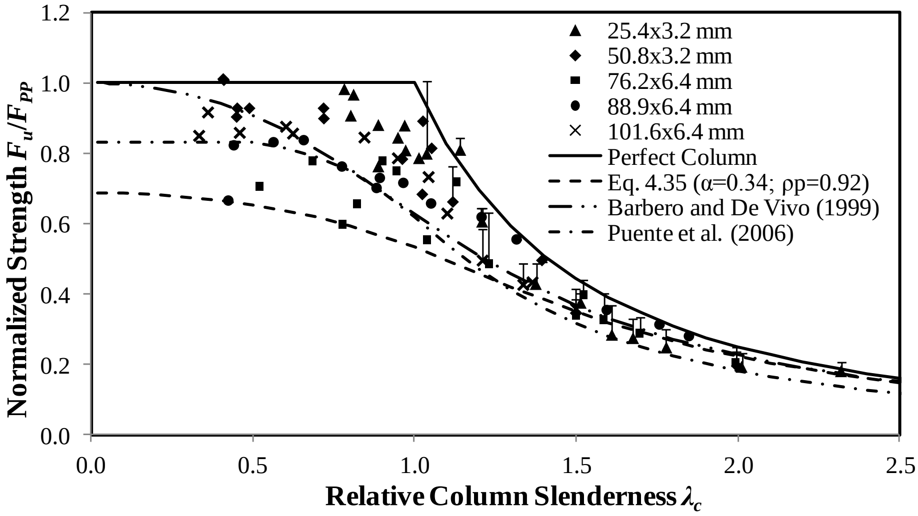

Figure 10. Experimental normalized ultimate stresses χ_c plotted against the relative column slenderness λ_c.

Representative failure modes are presented in Figure 11. The observed modes were mapped according to relative plate and column slenderness, as shown in Figure 12. From this ‘map’, important conclusions can be drawn: (i) long columns exhibited large deflections, regardless the wall slenderness; (ii) short columns failed either by crushing or local buckling followed by crushing; (iii) interaction between local and global buckling followed by crushing was observed for intermediate columns with $\lambda_p > 1$; and (iv) global buckling followed by crushing was observed for intermediate columns with $\lambda_p < 1$. In the ‘map’, the colors represent ranges of experimental strength reduction factor, ρ_c. It can be noted that lesser values of ρ_c were obtained for intermediate columns comprised of cross sections with intermediate walls.

a) 25.4x3.2 (λ = 0.89) showing crushing near mid-height which occurred following some degree of global buckling behaviour

b) 50.8x3.2 (λ = 0.72) showing kinking of compression face and rupture along web-flange interfaces associated with local buckling

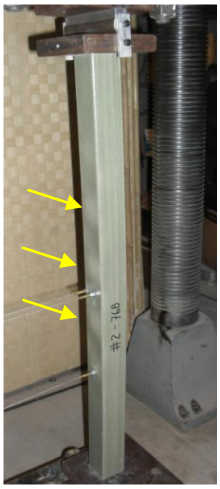

c) 50.8x3.2 (λ = 0.96) showing local buckling (arrows) and some degree of global buckling

d) 76.2x6.4 (λ = 0.78) crushing at end of specimen

e) 88.9x6.4 (λ = 1.76) showing global buckling behaviour typical of long columns

f) 101.6x6.4 (λ = 0.45) showing of local buckles (arrows)

Figure 11. Representative failure modes of column specimens.

6 CONCLUSIONS

In this work, a comprehensive approach to the behavior and strength of GFRP columns was presented. First, a perfect column model where independent failure modes by crushing, global buckling and local buckling is discussed. An expression to determine full-section local buckling critical stress for typical cross sections was introduced and the method was validated both numerically (FSM) and experimentally (stub column tests on I-sections). Then, a theoretical model of a real column with cross section comprised of real plates was developed. From this model, a column strength curve as a function of both plate and columns slenderness was derived. The expression was validated for square tubes after a set of tests on square tube columns having different lengths and sections. Some of the important conclusions are:

a. global buckling: as can be seen in Figure 9, Eq. 2 is in good agreement with experimental results, indicating that the referred equation is adequate to predict global buckling of GFRP columns;

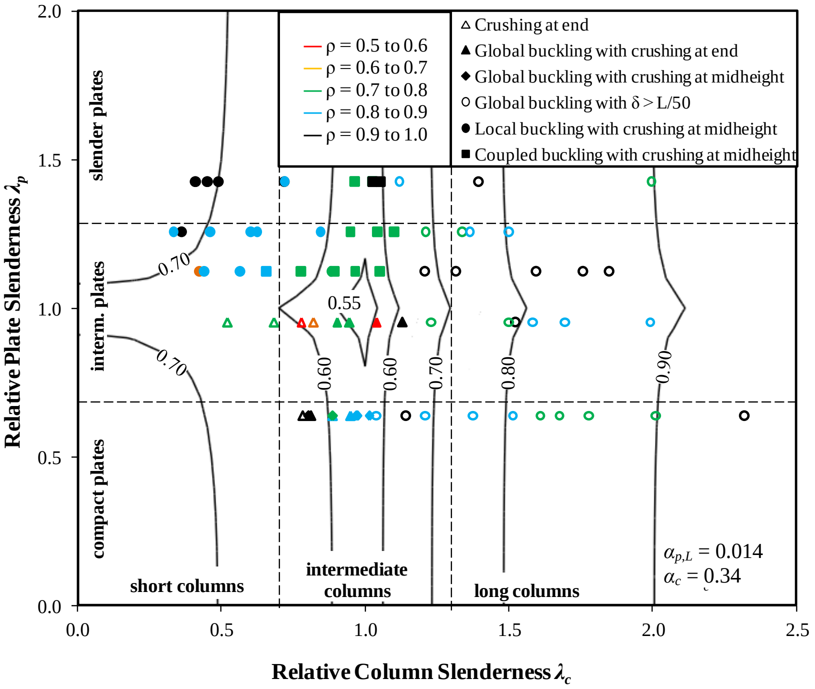

Figure 12 – Map of failure modes and column reduction factors according to column and plate slenderness.

b. local buckling: the critical buckling coefficients, k_{cr}, presented in Table 1 represent a more realistic and accurate representation of local buckling behavior of pultruded GFRP shapes than those presently adopted and proposed in current standards and guidelines (Figure 6). From the perspective of design, the conventional approach of assuming simply supported conditions at all plate interfaces (i.e.: Lekhnitskii's equations) is shown to be very conservative in all cases. the approach adopted for determining values of k_{cr} is very simple and led to good agreement within the range of typically available cross sections, with observed differences from FSM-calculated solutions of less than 10% in all cases (Table 2). Moreover, the approach used by CARDOSO *et al.* (2014c) to generate the proposed functions can be extended to other shapes and sections with non-uniform thickness and material properties. This approach can also be applied to evaluate local buckling of sections subject to flexure, as long as an adequate approximate function is selected.

c. real columns: the theoretical model for real columns was focused on sections comprised of simply supported walls, such as square tubes. However, it can be extended for other shapes and similar strength equations (Eq. 17) can be obtained, having different imperfection factors. Analysis of Eq.18 showed that the reduction of capacity is a function of both plate and column slenderness, with the greatest reduction of capacity occurring for $\lambda_c = \lambda_p = 1.0$; a column of intermediate slenderness comprised of intermediate plates. Numerical models can also be developed to confirm the model and to help understanding the behavior under different hypotheses (e.g. post buckling behavior and transverse shear effect).

d. local buckling tests on I-sections: the experimental study on I-sections, as well as the results of others (TOMBLIN and BARBERO, 1994, TURVEY and ZHANG, 2004), reported greater critical loads for short columns, which is attributed to the influence of specimen length and boundary conditions. Vinyl ester (VE) sections exhibited slightly higher elastic properties than polyester (PE), but no apparent differences were observed in the stub tests. To validate the proposed Eq. 3, more tests must be conducted: critical loads and experimental material properties must be reported. Testing longer columns with continuous lateral restraint to prevent global buckling would minimize the influence of end conditions resulting in reduced overstrength and closer agreement with the proposed equation. Other sections also need to be tested. A numerical analysis including actual boundary conditions would also be very clarifying.

e. compression tests on square tubes: it was shown that the proposed column curve (Eq. 17) represents adequately a lower bound for the compressive strength of GFRP tubes. However, additional column and stub tests must be carried out in order to determine reliable and representative imperfection factors that can be used for design purposes. The experiments confirmed that the greater reduction in capacity (ρ_c = 0.60) was observed for intermediate 76.2x6.4 tubes (λ_p = 0.94) of intermediate length (λ_c = 0.78 and λ_c = 1.04). This reduction is indicative of an interaction between crushing, local buckling and global buckling, as the predicted loads corresponding to each failure mode are similar.

ACKNOWLEDGEMENTS

All testing was conducted in the Watkins-Haggart Structural Engineering Laboratory (WHSEL) at the University of Pittsburgh. The authors gratefully acknowledge Bedford Reinforced Plastics for supplying the pultruded sections and Dr. Kent Harries and WHSEL staff for advice and support during research.

REFERENCES

ASCE Fiber Composites and Polymers Standards Committee (2010). Pre-standard for load & resistance factor design (LRFD) of pultruded fiber reinforced polymer (FRP) structures. Final Report submitted to American Composites Manufacturers Association (ACMA), ASCE. Reston VA USA.

Bank, L.C., and Yin, J. (1996). Buckling of orthotropic plates with free and rotationally restrained unloaded edges. *Thin Wall Struct*, v. 24, n. 1, p. 83-96.

Batista, E. M. (2004). Modelling buckling interaction, in Pignataro, M., Gioncu, V., editors, *Phenomenological and Mathematical Modelling of Structural Instabilities*, 470, pp. 135-194.

Barbero, E. J. (1998), Prediction of compression strength of unidirectional polymer matrix composites, *J Compos Mater*, 32(5), pp. 483-502.

Barbero, E.J. (2011). Introduction to composite materials design. 2nd Edition, CRC, Boca Raton, FL.

Barbero, E.J., De Vivo, L. (1999). Beam-column design equations for wide-flange pultruded structural shapes. *Journal of Composites for Construction*, v. 3, n. 4, p. 185-191.

Barbero, E. J., Makkapati, S., Tomblin, J. S. (1999), Experimental determination of the compressive strength of pultruded structural shapes, *Composites Science and Technology*, 59(13), pp. 2047-2054.

Barbero, E. J., Tomblin, J. (1994). A phenomenological design equation for FRP columns with interaction between local and global buckling. *Thin-Walled Structures*, v. 18, p. 117-131.

Bleich, F. (1952). Buckling Strength of Metal Structures. McGraw-Hill, New York.

Cardoso, D.C.T., Harries, K.A. and Batista, E.M. (2014a), On The Determination of Material Properties for Pultruded GFRP Sections, *Proceedings of the 7thInternational Conference on FRP Composites in Civil Engineering (CICE 2014)*, Vancouver, August.

Cardoso, D.C.T., Harries, K.A. and Batista, E.M. (2014b). Compressive strength equation for GFRP square tube columns. *Composites Part B: Engineering*, v. 59, p. 1-11.

Cardoso, D.C.T., Harries, K.A. and Batista, E.M. (2014c). Closed-form equations for local buckling of pultruded thin-walled sections. *Thin-Walled Structures*, v. 79, p. 16-22

Cardoso, D.C.T., Harries, K.A. and Batista, E.M. (2015). Compressive local buckling of pultruded GFRP I-sections: development and numerical/experimental evaluation of an explicit equation. *Journal of Composites for Construction*, v. 19, n. 2, p. 8-15.

Clarke, J. L. (1996). Structural design of polymer composites: EUROCOMP design code and handbook. Taylor & Francis, London.

CNR, National Research Council of Italy (2008). CNR-DT 205/2007: Guide for the design and construction of structures made of thin FRP pultruded elements. Rome.

CRCJ, Column Research Committee of Japan (1971). Handbook of Structural Stability. Corona, Tokyo.

Dutheil J. (1961). La prise en compte des imperfections inévitables dans la détermination des systèmes hyperstatiques en acier sollicités au flambement. *Mémoires AI PC*, 21, 1961, pp. 61-94.

Fleck, N. A. (1997). Compressive failure of fiber composites, in Hutchinson, J.W., Wu, T.Y., editors, Advances in Applied Mechanics, 33, pp. 43-117.

Gray, E. F. (1984). Structural plastics design manual. ASCE, New York.

Hashem, Z. A., Yuan, R. L. (2001). Short vs long column behavior of pultruded glass-fiber reinforced polymer composites. *Construction and Building Materials*, v. 15, p. 369-378.

Hewson, P. J. (1978). Buckling of pultruded glass fibre-reinforced channel sections. *Compos.*, v. 9, n. 17, p. 56-60.

Kollár, L.P. (2002). Buckling of unidirectionally loaded composite plates with one free and one rotationally restrained unloaded edge. *J. Struct. Eng.*, v. 128, n. 9, p. 1202-1211.

Kóllar, L.P. (2003). Local buckling of fiber reinforced plastic composite structural members with open and closed cross sections. *J. Struct. Eng.*, v. 129, n. 11, p. 1503-1513.

Kroll, W.D., Fisher, G.P., and Heimerl, G.J. (1943). Charts for calculation of the critical stress for local instability of columns with I-, Z-, channel, and rectangular-tube section. No. NACA-WR-L-429, National Aeronautics and Space Admin Langley Research Center, Hampton, VA.

Lane, A. and Mottram, J.T. (2002). The influence of modal coupling upon the buckling of concentrically PFRP columns. *Inst Mech Engrs Part L: J Mater*, Des Appl, v. 216, n. 12, p. 133–44.

Lee, D.J. and Hewson P.J. (1978). The use of fiber-reinforced plastics in thin-walled structures. Proc. Stability Problems in Engineering Structures and Composites, Applied Science, London.

Lekhnitskii, S.G. (1968). Anisotropic plates. Gordon and Breach Science Publishers, New York.

Li, Z., Schafer, B.W. (2010). Buckling analysis of cold-formed steel members with general boundary conditions using CUFSM: conventional and constrained finite strip methods.

Proceedings of the 20th Int. Spec. Conf. on Cold-Formed Steel Structures, St. Louis, MO, November.

Lundquist, E. E., Stowell, E. Z., and Schuette E. H. (1943). Principles of moment distribution applied to stability of structures composed of bars or plates. National Advisory Committee for Aeronautics.

Puente, I., Insausti. A., Azkune, M. (2006), Buckling of GFRP columns: an empirical approach to design. *Journal Composites for Construction*, v. 10, n. 6, p. 529-537.

Qiao, P., Shan, L. (2005). Explicit local buckling analysis and design of fiber–reinforced plastic composite structural shapes. *Composite Structures*, 70, n. 4, pp. 468-483.

Southwell, E. V. (1932). On the analysis of experimental observations in problems of elastic stability. Proceedings of Royal Society of London, v. 135, p. 601-616.

Timoshenko S.P., and Gere J.M. (1961). Theory of elastic stability. McGraw-Hill, New York.

Turvey, G.J., Zhang, Y. (2004). Local buckling of axially compressed, pultruded GRP, WF-section, short columns - comparison of experimental and FE analysis buckling loads. *Applied Mechanics and Materials*, v. 1, p. 87-92.

Zahn, J.J. (1992). Re-examination of Ylinen and other column equations, interaction of rupture and buckling in wood members. *ASCE J. Struct. Eng.*, v. 118, n. 10, p. 2716-28.

Zureick, A., Scott, D. (1997). Short-term behavior and design of fiber-reinforced polymeric slender members under axial compression. *Journal Composites for Construction*, v. 1, n. 4, p. 140-149.

Zureick, A., Steffen, R. (2000). Behavior and design of concentrically loaded pultruded angle struts. *ASCE Journal of Structural Engineering*, v. 126, n. 3, p. 406-416.

Seangatith, S., Sriboonlue, W. (1999). Axially loaded glass-fiber reinforced plastic composite columns. Seventh East Asia-Pacific Conference on Structural Engineering & Construction, Kochi, Japan, p. 1307-1312.

Seangatith, S. (2004). GFRP box columns with different supports subjected to axial compression. In Proc. 9th National Convention on Civil Engineering, Phetchaburi, Thailand.